# ANALYZING AND PREDICTING THE EXTRATROPICAL TRANSITION OF TROPICAL CYCLONES.

by

Elizabeth A. Ritchie[1], J. S. Tyo[1], and O. Demirci[2]

[1]University of Arizona
[2]University of New Mexico

## 1. INTRODUCTION

Extratropical transition (ET) is a process that a tropical cyclone can undergo as it moves to higher latitudes over colder seas and interacts with the midlatitude regime. The resulting extratropical cyclone can be powerful with heavy precipitation to the left of track and a large extent of gale-force-winds to the right of track. These large asymmetries produce significant hazards to coastal settlements and maritime activities that range from heavy precipitation, large waves, high winds, and even fire weather. The whole transition process typically takes 48-72 hours to be completed (Klein et al. 2000).

In the most basic sense, there are two possible outcomes: dissipation or intensification of the combined system. These two classes of tropical cyclones behave very similarly during the early stages of extratropical transition. Thus, the end result of this transition is very hard to predict accurately even with full-physics atmospheric prediction systems such as the Navy's Operational Global Assimilation and Prediction System (NOGAPS). Although there are many factors involved in the process, research has shown that the reintensification of the extratropical cyclone results primarily from its interaction with a midlatitude trough (e.g., Ritchie and Elsberry 2003). Thus, the end result of extratropical transition may depend more on the phasing between the tropical cyclone and the trough it moves into rather than the details of the tropical cyclone structure (Ritchie and Elsberry 2007).

Here we present results from a multi-stage, pattern-recognition technique to predict the simplest of ET outcomes: whether an ETing system will reintensify or dissipate after ET. To date the projection pursuit (PP) system uses NOGAPS analyses as input to a statistical technique that separates the discriminating large scale factors associated with reintensifying or dissipating ET cases. Using this PP technique, the most effective set of variables that discriminate dissipation and reintensification can be investigated and prediction of ET outcome accomplished. Our aim is to achieve this prediction at least 24 hours in advance of the ET time (defined later) after which reintensification occurs.

First, we describe the data in Section 2, and then explain the details of the technique in Section 3. In Section 4.1, we present the results obtained using individual variables, and the corresponding patterns contributing to intensification are analyzed in Section 4.2. In Section 4.3, we compare the performance of individual variables with coupled pairs of variables and we present our conclusion and future plans in Section 5.

## 2. DATA

The data used for this research are the NOGAPS analyses every 12 hours from 48 hours prior to a predetermined ET time to 48 hours subsequent. The analyses were obtained from the Master Environmental Library (MEL). Additional data sources include cloud drift winds provided by the Space Science and Engineering Center at the University of Wisconsin. Basic and derived variables are shown in table 1 and include geopotential height (m), relative humidity (%), temperature (K), U, and V components of the wind (m/s), sea-level pressure (hPa), sea-surface temperature (K), equivalent potential temperature (K), cloud-drift winds (m/s), vorticity (/s), and divergence (/s).

All analyses have a spatial resolution of 1° latitude-longitude and time resolution of 12 hours. The individual fields were centered on the tropical cyclone locations determined by the

| | Basic Variables | | | | | | | Derived variables | | | | |
|---|---|---|---|---|---|---|---|---|---|---|---|---|
| | HGT | RH | TMP | U | V | SLP | SST | $\theta_e$ | U* | V* | Vor | Div |
| **100 hPa** | ✓ | ✓ | ✓ | ✓ | ✓ | | | ✓ | ✓ | ✓ | ✓ | ✓ |
| **200 hPa** | ✓ | ✓ | ✓ | ✓ | ✓ | | | ✓ | ✓ | ✓ | ✓ | ✓ |
| **300 hPa** | ✓ | ✓ | ✓ | ✓ | ✓ | | | ✓ | ✓ | ✓ | ✓ | ✓ |
| **500 hPa** | ✓ | ✓ | ✓ | ✓ | ✓ | | | ✓ | ✓ | ✓ | ✓ | ✓ |
| **700 hPa** | ✓ | ✓ | ✓ | ✓ | ✓ | | | ✓ | ✓ | ✓ | ✓ | ✓ |
| **850 hPa** | ✓ | ✓ | ✓ | ✓ | ✓ | | | ✓ | ✓ | ✓ | ✓ | ✓ |
| **925 hPa** | ✓ | ✓ | ✓ | ✓ | ✓ | | | ✓ | ✓ | ✓ | ✓ | ✓ |
| **1000 hPa** | ✓ | ✓ | ✓ | ✓ | ✓ | | | ✓ | ✓ | ✓ | ✓ | ✓ |
| **Surface** | | | | | | ✓ | ✓ | | | | | |

Table 1: Variables used in the PP Algorithm. On the left: NOGAPS analyses obtained directly from MEL at various pressure levels. On the right: Variables derived from the NOGAPS analyses and cloud drift wind data.

Joint Typhoon Warning Center. The analyses were then interpolated to 61° longitude and 51° latitude grids at each individual time.

The ET time was defined as the time when the tropical cyclone first appeared as an open wave on the midlatitude baroclinic zone in the NOGAPS 500-mb height analyses. This was subjectively determined for each case. When compared with other definitions of ET (e.g., Harr et al. 2000; Klein et al. 2000; Hart 2003) there was little difference in the ET time during the period of interest. Any reintensification occurs subsequent to this time, so that any predictive value prior to this time is useful.

A total of 97 tropical cyclone ET cases were analyzed from the years 1997-2005. Seventy storms from the years 1997-2003 were used as training data for the PP algorithm. These included 36 intensifying and 34 dissipating cases. The test group included a total of 27 storms (14 intensifiers and 13 dissipaters) from the later years (2004-2005).

## 3. ANALYSIS

The basic PP algorithm is described in Demirci et al. (2007). The algorithm is extended here to include multiple variables in the analysis by replacing the initial empirical orthogonal function (EOF) analysis by either singular vector decomposition (SVD) or an extended EOF (EEOF) analysis.

In the case of SVD or EEOF analysis the original single variable *m x N* matrix, $\boldsymbol{X_1}$, which contains a single analysis field (e.g., 500-mb heights) for *N* training cases, is combined with a second *n x N* matrix, $\boldsymbol{X_2}$, containing a second variable (e.g., 200-mb temperature) for all *N* training cases. Note that $\boldsymbol{X_2}$ is not required to have the same dimensionality as $\boldsymbol{X_1}$, in this analysis. Were we to do separate EOF analyses on these two matrices, we would obtain the corresponding covariance matrices $\boldsymbol{X_1X_1^T}$ and $\boldsymbol{X_2X_2^T}$. These can be decomposed into the form

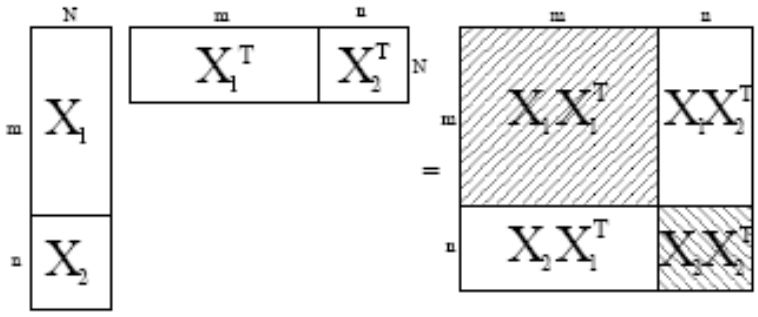


Figure 1: Covariance matrix for matrices $\boldsymbol{X_1}$ and $\boldsymbol{X_2}$. *N* is the number of tropical cyclone cases, *m* and *n* represent the number of grid points each analysis field includes (e.g. 61 x 51 = 3111).

$$C_1 = X_1X_1^T = V_1\Lambda_1V_1^{-1} = V_1\Lambda_1V_1^{-1}$$

$$C_2 = X_2X_2^T = V_2\Lambda_2V_2^{-1} = V_2\Lambda_2V_2^{-1}.$$

Assuming that the TC observations are independent (matrices $X_1$ and $X_2$), then $C_1$ and $C_2$ are symmetric and positive definite. The $\Lambda_i$'s are diagonal and contain the eigenvalues. The matrices $V_1$ and $V_2$ contain the eigenvectors, which are orthogonal to each other. By combining them together we obtain the two-variable ($m$+$n$) x ($m$+$n$) covariance matrix as shown in Figure 1, which includes $X_1 X_1^T$, $X_2 X_2^T$, $X_1 X_2^T$, and $X_2 X_1^T$. This method is referred as EEOF analysis and the entire covariance matrix on the right side of Figure 1 is utilized in the decomposition process. We can also utilize just the cross-coupled patterns between the two variables. These are shown in Figure 1 as the non-shaded parts of the entire covariance matrix. If just these cross-coupled patterns are used, the analysis is an SVD analysis. Although not as much information is used in an SVD analysis compared to an EEOF analysis, the results are similar and robust. The computational savings in the SVD analysis make it an attractive alternative to the EEOF analysis.

After SVD or EEOF analysis is applied to the variables, the rest of the PP algorithm as described in Demirci et al. (2007) is run. The final outcome is a one-dimensional decision space in which the algorithm can be used to objectively determine whether a testing storm falls into a dissipating or intensifying class of ET storms.

## 4. RESULTS

### 4.1 Spatial Results with individual variables

Initially, the NOGAPS analyses for geopotential height, temperature, relative humidity, equivalent potential temperature, u, v, vorticity, and divergence were used in the single-variable version of the PP algorithm (using EOF analysis). The performances of each variable at different pressure levels in the atmosphere were investigated using the test group from 2004 and 2005. Figure 2 shows the individual performances for geopotential height and divergence at 8 pressure levels in the atmosphere at each time step from 48 hours prior, to 48 hours subsequent to the ET time.

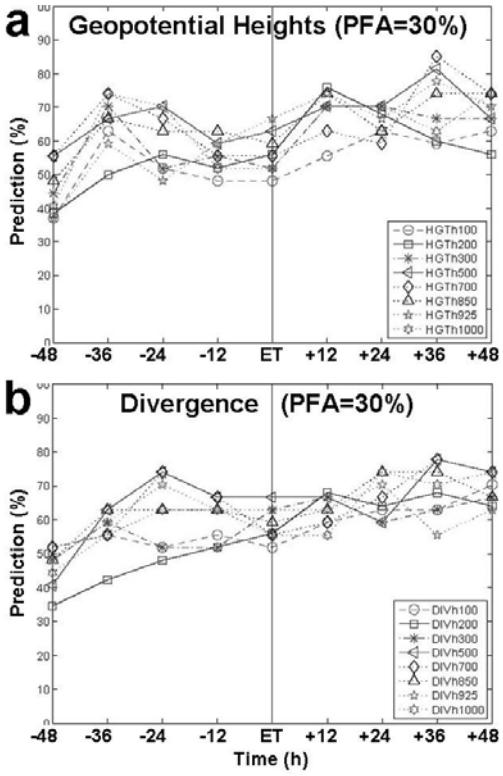


Figure 2: Overall percent prediction for 27 test cases from 2004 and 2005 using: a) geopotential height analyses; and b) divergence at various levels in the atmosphere.

Overall, for the geopotential height variable, the 500-hPa level performs most consistently with a prediction rate of 60-70% up to 36 hours prior to the ET time at a threshold probability of false alarms ($P_{FA}$) of 30% (Fig. 2a). Temperature performed similarly to heights with best performance in the lower levels of the atmosphere (not shown). Both lower-level vorticity (not shown) and middle-level divergence (Fig. 2b) performed near 80% at times prior to ET.

### 4.2 Analysis of spatial results

The final step in the PP algorithm is to find the direction in 10-dimensional space that optimizes the separation between the dissipating and reintensifying groups of tropical cyclones (Demirci et al. 2007). By investigating the spatial patterns of the end points of this separation line, we can analyze the differences in various fields that discriminate the two classes of tropical cyclones.

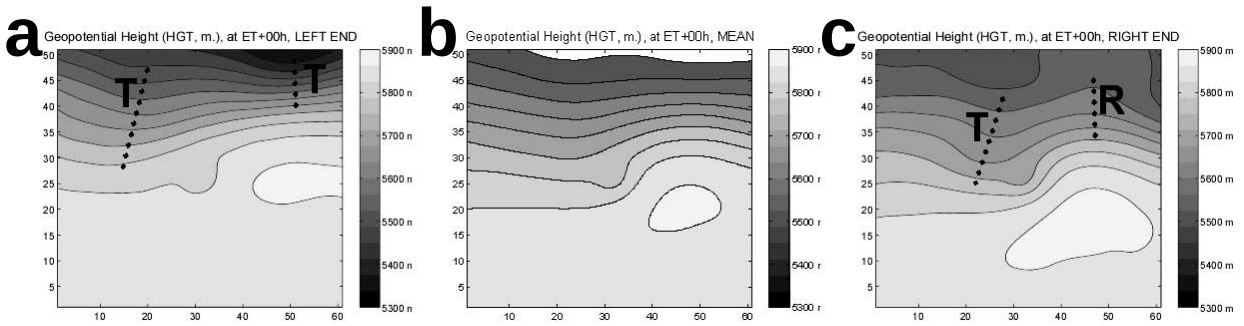


Figure 3: Reconstructed geopotential height end images at 500 hPa of the maximum separation line at ET time: a) negative end image represents dissipaters; b) mean image; and c) positive end image, which represents reintensifying storms.

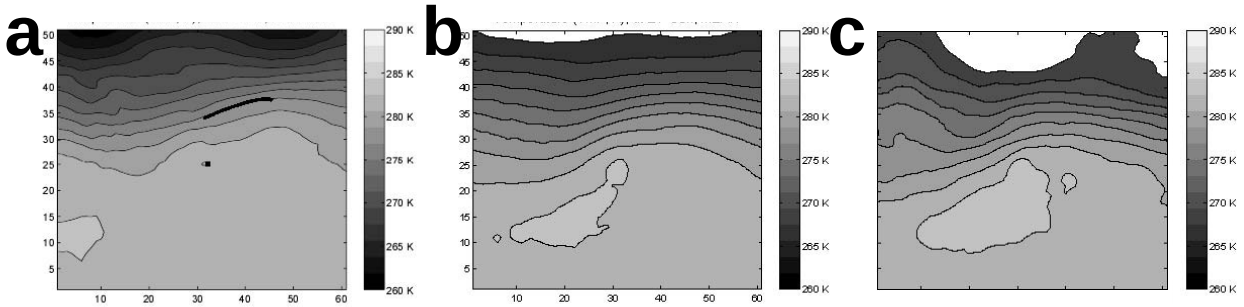


Figure 4: Reconstructed temperature end images at 700 hPa of the maximum separation line at ET time: a) negative end image represents dissipaters; b) mean image; and c) positive end image, which represents reintensifying storms.

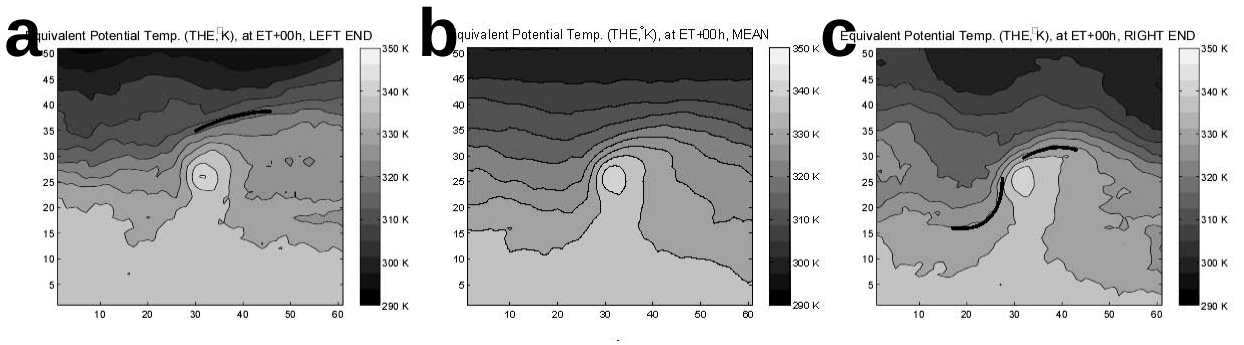


Figure 5: Reconstructed equivalent potential temperature ($\theta_e$) end images at 700 hPa of the maximum separation line at ET time: a) negative end image represents dissipaters; b) mean image; and c) positive end image, which represents reintensifying storms.

Figure 3 shows the reconstructed end analyses for 500-hPa geopotential heights at the ET time. Figure 3c indicates a strong trough-ridge pattern in the TC location with the TC located between the axes of these patterns and underneath the divergence maximum associated with the upper-level jet. Figure 3a represents a more zonally oriented flow with the northwest trough located farther away from the TC compared to Figure 3c. In Figure 3a the primary midlatitude circulation feature is the trough located to the northeast of the TC similar to the northeast pattern determined by Harr et al. 2000. The same behavior was seen in all layers with consistent progression at different times.

The maximum separation direction end images for the temperature analyses at the ET time for the 700-hPa level can be seen in Figure 4. The intensifying end, Figure 4c, has an asymmetry to the south of the TC. The contours are more closely spaced to the northeast of the TC than to the northwest indicating that the change in temperature is more rapid in the northeast. This is an indication of warm frontal formation (strong horizontal temperature contrasts). Frontal formation to the northeast of the TC is closer to the TC in the positive end compared to the negative (dissipating) end. The pattern indicates the deformation of the low-level baroclinic zone due to the tropical cyclone circulation similar to that described by Schultz et al. (1998). The deformation in Figure 4a is far less pronounced indicating a weaker frontal development pattern.

The spatial patterns at the 700-hPa level for equivalent potential temperature ($\theta_e$) analyses are presented in Figure 5. The pattern is similar to that in Figure 4 with more pronounced formation of surface fronts in the reintensifying end image than the dissipating end image.

### 4.2 Performance using coupled patterns

The forecasting performance of the system can be increased further by using the coupled patterns between individual variables. In the PP algorithm, the EOF analysis stage is replaced by either SVD or EEOF as described in section 3. Every 2-variable combination has been calculated and examined. We present some of these results and compare with the performance of the individual variables.

The cross-coupled performance of temperature and divergence using EEOF with a threshold $P_{FA}$ = 20% at the ET time is presented in Table 2. The prediction performances higher than 70% are highlighted with gray. The first column and row include the forecasting performance of the variables alone. It can be seen that individually, 700-hPa temperature analyses and 300-hPa and 500-hPa divergence analyses perform better than other levels. When coupled modes are used, there is some improvement. With one exception, there is a counter-intuitive result that low-level temperature coupled with low-level divergence patterns gives the better performance. The exception is 850-hPa temperature coupled with 200-hPa divergence, which gives a performance of 72% at ET time, an improvement over each individual variable.

The cross-coupled performance of temperature and divergence using SVD is presented in Table 3. The prediction performances higher than 70% are again highlighted in gray. Similar behavior is observed using the SVD analysis to the EEOF analysis. Higher predictions are obtained, but again, the cross-coupling is unexpectedly between low-level temperature and mid- to low-level divergence with performances increased to 80% in one case.

The performances presented in Tables 2 and 3 indicate that addition of a second variable to the PP technique may increase the detection performance and provide more stability. Using other false-alarm thresholds and other variables better results can be obtained. For example, decreasing the false-alarm threshold to 10% can bring prediction rates up to 78% for 500-hPa temperature cross-coupled with 700-, 850, or 925-hPa divergence. We are still in the process of analyzing, assessing and measuring these performances.

## 5. CONCLUSIONS

We have presented a multi-stage projection pursuit algorithm and applied it to various NOGAPS analyses to investigate how cross-coupling between different variables and different levels of the atmosphere can improve discriminating between two basic classes of ET: dissipaters and reintensifiers. The technique has provided encouraging results and further analysis of how the cross-coupled variables impact ET is still being conducted. In addition, analysis of the predictive results of the cross-coupled patterns is being undertaken to further improve the algorithm, We are extending various components

of the PP algorithm to make it a true forecasting system and hope to begin real-time testing in the 2008 season.

**REFERENCES:**


Demirci, O., J. S. Tyo, and E. A. Ritchie 2007: Spatial and spatiotemporal projection pursuit techniques to predict the extratropical transition of tropical cyclones. *IEEE Trans. Geoosciences and remote sensing.* **45,** 418-424.

Harr,, P. A., R. L. Elsberry, and T. F. Hogan, 2000: Extratropical transition of tropical cyclones over the western North Pacific. Part II: The impact of midlatitude circulation characteristics," *Mon. Wea. Rev.*, **128**, 2634–2653.

Hart, R. E., 2003: A cyclone phase space derived from thermal wind and thermal asymmetry. *Mon. Wea. Rev.,* **131,** 585-616.

Klein, P. M., P. A. Harr, and R. L. Elsberry, 2000: Extratropical Transition of Western North Pacific Tropical Cyclones: An Overview and Conceptual Model of the Transformation Stage. *Wea. and Fore.,* **15,** 373–395.

Ritchie, E. A., and R. L. Elsberry 2003: Simulations of the extratropical transition of tropical cyclones: Contributions by the midlatitude upper-level trough to reintensification. *Mon. Wea. Rev.,* **131,** 2112-2128.

Ritchie, E. A., and R. L. Elsberry 2007: Simulations of the extratropical transition of tropical cyclones: Phasing between the upper-level trough and tropical cyclone. *Mon. Wea. Rev.,* **135**, 862–876.

Schultz, D. M., D. Keyser, and L. F. Bosart 1998: The Effect of Large-Scale Flow on Low-Level Frontal Structure and Evolution in Midlatitude Cyclones. *Mon. Wea. Rev.,* **126**, 1767–1791.



**ACKNOWLEDGEMENTS:** This research was sponsored by the Office of Naval Research marine meteorology program and comprises part of the dissertation research of Dr. O. Demirci.


| EEOF | | | Temperature (K) | | | | | |
|---|---|---|---|---|---|---|---|---|
| | | | 300 hPa | 500 hPa | 700 hPa | 850 hPa | 925 hPa | 1000 hPa |
| | | | 44.4 | 59.3 | 70.4 | 66.7 | 55.6 | 51.9 |
| | 100 hPa | 51.9 | 51.9 | 55.6 | 66.7 | 66.7 | 59.3 | 51.9 |
| | 200 hPa | 44.0 | 56.0 | 48.0 | 48.0 | 72.0 | 56.0 | 52.0 |
| | 300 hPa | 74.0 | 48.1 | 55.6 | 55.6 | 70.4 | 44.4 | 48.1 |
| | 500 hPa | 81.5 | 48.1 | 59.3 | 66.7 | 48.1 | 63.0 | 55.6 |
| | 700 hPa | 59.3 | 44.4 | 66.7 | 63.0 | 63.0 | 59.3 | 48.1 |
| | 850 hPa | 63.0 | 55.6 | 59.3 | 74.1 | 63.0 | 66.7 | 44.4 |
| | 925 hPa | 51.9 | 48.1 | 70.4 | 63.0 | 70.4 | 59.3 | 55.6 |
| | 1000 hPa | 59.3 | 44.4 | 66.7 | 70.4 | 66.7 | 63.0 | 51.9 |

Table 2: EEOF prediction performance using 2004-2005 in the test group, and 1997-2003 in the training. False alarm rate is set at 20% and the results are shown for the ET time.

| SVD | | | Temperature (K) | | | | | |
|---|---|---|---|---|---|---|---|---|
| | | | 300 hPa | 500 hPa | 700 hPa | 850 hPa | 925 hPa | 1000 hPa |
| | | | 44.4 | 59.3 | 70.4 | 66.7 | 55.6 | 51.9 |
| | 100 hPa | 51.9 | 44.4 | 44.4 | 66.7 | 66.7 | 59.3 | 59.3 |
| | 200 hPa | 44.0 | 44.0 | 72.0 | 56.0 | 64.0 | 52.0 | 48.0 |
| | 300 hPa | 74.0 | 40.7 | 55.6 | 66.7 | 63.0 | 51.9 | 33.3 |
| | 500 hPa | 81.5 | 44.4 | 55.6 | 70.4 | 70.4 | 59.3 | 48.1 |
| | 700 hPa | 59.3 | 51.9 | 55.6 | 74.1 | 66.7 | 63.0 | 51.9 |
| | 850 hPa | 63.0 | 40.7 | 63.0 | 81.5 | 63.0 | 70.4 | 55.6 |
| | 925 hPa | 51.9 | 59.3 | 59.3 | 63.0 | 70.4 | 55.6 | 59.3 |
| | 1000 hPa | 59.3 | 44.4 | 63.0 | 66.7 | 66.7 | 55.6 | 48.1 |

Table 3: SVD prediction performance using 2004-2005 in the test group, and 1997-2003 in the training. False alarm rate is set at 20% and the results are shown for the ET time.